PROCEEDINGS of the
23rd International Congress on Acoustics
9 to 13 September 2019 in Aachen, Germany

Analysis and optimisation of an active noise control system as a potential acoustic metamaterial building block

Joe Tan1[(1)], Jordan Cheer[(2)] and Stephen Daley[(3)]

[(1)]University of Southampton, United Kingdom, j.tan@soton.ac.uk
[(2)]University of Southampton, United Kingdom,
[(3)]University of Southampton, United Kingdom,

ABSTRACT

Active Noise Control (ANC) systems have been employed in a variety of applications to provide high performance noise control at low frequencies, within a lightweight and compact package. Recently, acoustic metamaterials (AMM) have been proposed and demonstrated as an alternative approach to achieving high levels of noise control. AMM are engineered structures that consist of an array of subwavelength unit cells, which exhibit behaviour not seen in conventional materials. For example, passive resonators have been designed to achieve negative effective material properties and manipulate wave propagation. These AMMs, however, typically have narrow band gaps, where wave propagation is suppressed. When acting as an AMM, ANC systems have been shown to improve performance, tuneability and adaptability, but physical insights have generally been limited. Therefore, this paper investigates the effects of traditional ANC on the effective material properties and shows physical insight through an analysis of the wave propagation within a one-dimensional duct system. The active unit cell has then been optimised to directly minimise the effective material properties and a corresponding physical analysis has been presented.

Keywords: Active Noise Control, Acoustic Metamaterials, negative density, negative bulk modulus.

1 INTRODUCTION

Active noise control (ANC) is an advanced technology that provides high levels of noise control at low frequencies whilst maintaining a lightweight and compact package, which is difficult to achieve using traditional passive control treatments. ANC also has the capability to adapt to changes in the acoustic environment, as well as the ability to shape and manipulate the sound quality. In recent years, an alternative approach to achieve high levels of noise control at low frequencies within a lightweight and compact package has been developed through the design of acoustic metamaterials (AMMs). AMMs achieve high performance noise control by designing an engineered structure consisting of an array of subwavelength unit cells. Since the unit cells are subwavelength, the entire structure is considered to be a homogeneous medium with an effective density and bulk modulus that can take on positive, negative and even zero values. These dynamic material properties allow acoustic metamaterials to achieve behaviour that is not seen in conventional materials, such as near-zero refractive index [1, 2] and negative effective density [3, 4] or bulk modulus [5, 6] or even both [7, 8]. The greater range of material properties that are available to acoustic metamaterials allow these materials to not only control the transmission of sound, but, they have also shown the potential to be used in more novel technologies, for example, superlenses [9, 10] and acoustic cloaking [11, 12]. Passive acoustic resonators have shown the ability to achieve negative effective material properties, however, these materials typically have narrow band gaps and moderate performance due to losses associated with the passive resonators [4, 13]. To overcome the limitations of passive AMMs, active control has been combined with passive resonators to increase the level of performance and width of the band gaps whilst increasing the adaptability and tuneability of these materials [14, 13].

Although a variety of active AMMs have been proposed, the active control systems employed within these materials typically differ from traditional ANC systems. That said traditional ANC strategies have been used in recent years in the context of AMM to control the transmission of sound using active Helmholtz resonators

[15] and have also been used to minimise the scattered sound field to create an active acoustic cloak [16]. Furthermore, [17] also identified the links between traditional active control systems and the behaviour of AMMs.

The work presented in this paper will further investigate the effects of traditional ANC systems on the effective material properties whilst providing physical insight how the active control systems manipulate wave propagation within a one-dimensional anechoically terminated duct. Using the same one-dimensional duct system, this paper will also investigate whether active control can be used to directly control the effective material properties using an optimisation procedure. Section 2 presents the one-dimensional system used in this study. Section 3 describes the theoretical formulations of the traditional active control strategy considered in this study and presents a simulation-based investigation of its performance resulting effective material properties and physical behaviour. Section 4 describes the optimisation procedure used to minimise the effective material properties using the active control systems and also presents the results of simulations following the same form as in Section 3. Finally, Section 5 presents the conclusions.

2 SYSTEM SETUP

Figure 1 shows the one-dimensional duct system used throughout this study. This figure shows that the one-dimensional system contains a primary source at one end and an anechoic termination at the other end and the active control unit is placed at the centre of the duct with two pressure microphones located either side of the active control unit. The traditional ANC strategy considered in this study is the minimisation of downstream pressure using three different source configurations; a single monopole, dipole and pair of monopole control sources. Also, using the system shown in Figure 1, a single monopole control source has been optimised to minimise the effective bulk modulus and a dipole control source has also been optimised to minimise the effective density.

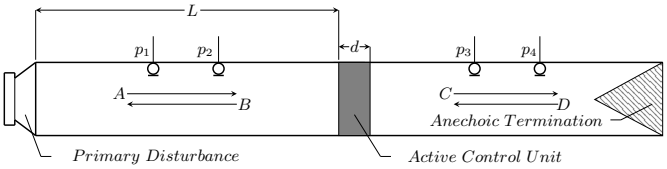

Figure 1. The anechoically terminated duct setup showing the primary disturbance source, the four pressure microphone positions and the location of the active control unit.

The frequency range of interest has been restricted to low frequencies, where the wavelength is much larger than the diameter of the duct and, thus, plane wave propagation can be assumed. The total sound pressure at a point, x, in the duct can be represented by the linear superposition of the pressures due to the primary, $p_p(x)$, and secondary, $p_s(x)$, sources and can be written as

$$p(x) = p_p(x) + p_s(x) \tag{1}$$

where x is the coordinate position in the duct. Following the assumption of plane wave propagation, the sound pressure due to the primary source can be expressed as

$$p_p(x) = \frac{\rho_0 c_0}{2S} q_p \mathrm{e}^{-\mathrm{j}k|x+L|} \tag{2}$$

where ρ_0 and c_0 are the density and speed of sound in air, S is the cross-sectional area of the duct, L is the distance between the primary source and active control unit, k is the wavenumber and q_p is the primary source strength. The following sections will describe the formulation to obtain the secondary source sound field required to control the downstream pressure and the effective material properties of the fluid medium.

3 MINIMISATION OF DOWNSTREAM PRESSURE

There has been a wide variety of active control strategies developed for various applications, however, for the one-dimensional duct control problem the most fundamental active controller aims to minimise the downstream propagation of the acoustic wave. In the following sections, this control strategy will be formulated for different secondary source arrangements before the behaviour of these arrangements is evaluated.

3.1 Control Strategy Formulation

The first secondary source arrangement that will be considered here is a single monopole control source located at $x = 0$ in the duct and driven to minimise the downstream pressure. Using the formulation described in [17], the optimal secondary source strength in this case is

$$q_s = -q_p \mathrm{e}^{-\mathrm{j}kL}. \tag{3}$$

The second case considered in this study is a dipole control source and the sound pressure produced by this source in the upstream and downstream sections of the duct can be written as [17]

$$p_s(x) = -\frac{f}{2S}\mathrm{e}^{-\mathrm{j}k|x|}, \quad \text{for} \quad x < 0 \quad \text{and} \quad p_s(x) = \frac{f}{2S}\mathrm{e}^{-\mathrm{j}k|x|}, \quad \text{for} \quad x > 0 \tag{4}$$

where f is the dipole force. Using the formulation described in [17] in this case, the optimal dipole force is

$$f = \rho_0 c_0 \mathrm{e}^{-\mathrm{j}kL}. \tag{5}$$

When minimising the downstream pressure, the single monopole and dipole control sources increase the sound pressure in the upstream section of duct. To overcome this limitation, a pair of monopole control sources can be used to minimise the downstream pressure in the duct whilst producing zero upstream sound radiation. In this case, the first monopole source is located at $x = 0$ and the second monopole source is located at $x = d$, as shown in Figure 1. To achieve zero upstream sound radiation, the first monopole source strength, q_{s1}, must be related to the second monopole source strength, q_{s2}, by

$$q_{s1} = -q_{s2}\mathrm{e}^{-\mathrm{j}kd}. \tag{6}$$

Using the formulation described in [17] in this case, the second monopole control source strength that minimises the downstream pressure is then given by

$$q_{s_2} = -q_p \frac{\mathrm{e}^{-\mathrm{j}kL}}{2\mathrm{j}\sin(kd)}. \tag{7}$$

3.2 Performance Metrics

The performance of each secondary source configuration optimised using the downstream pressure minimisation control strategy has been assessed using the transmission and reflection coefficients and dissipated energy. Additionally, the effective material properties have been calculated using the retrieval method described in [18] so that the behaviour of the ANC strategies can be linked to the metamaterial literature. Using the pressure at the four microphones shown in Figure 1, the complex wave amplitudes of the four travelling waves can be calculated, which are indicated by the coefficients A to D shown in Figure 1. The performance metrics can then be obtained using the complex wave amplitudes and they can be expressed as

$$T = \frac{C}{A}, \quad R = \frac{B}{A} \quad \text{and} \quad E_d = 1 - (|R|^2 + |T|^2) \tag{8}$$

where T is the transmission coefficient, R is the reflection coefficient and E_d is the dissipated energy.

Using the transmission and reflection coefficients, the effective refractive index, n_{eff}, and impedance, z_{eff}, can also be calculated as [18]

$$n_{eff} = \frac{-\mathrm{j}\ln(\phi) + 2\pi m}{kd} \quad \text{and} \quad z_{eff} = \frac{\rho_0 c_0 q}{1 - 2R + R^2 - T^2} \tag{9}$$

where

$$q = \sqrt{(R^2 - T^2 - 1)^2 - 4T^2}, \quad \phi = \frac{1 - R^2 + T^2 + q}{2T}$$

and m is the branch number. The effective refractive index and impedance can then be used to calculate the effective material properties, which can be expressed as [19]

$$\rho_{eff} = \frac{n_{eff} Z_{eff}}{c_0} \quad \text{and} \quad B_{eff} = \frac{Z_{eff} c_0}{n_{eff}}, \tag{10}$$

where ρ_{eff} is the effective density and B_{eff} is the effective bulk modulus of the fluid medium. From Eq. 9, it can be seen that the refractive index and impedance contain multiple solutions, which can lead to the incorrect selection of the effective material properties. In order to obtain the correct refractive index, the algorithm described in [20] has been used to estimate the correct branch number, which in turn selects the correct effective material properties.

3.3 Results

The effective material properties and performance metrics for each source configuration have been calculated using the procedure outlined above and these results are presented in Figure 2. From these results, it can be seen that the single monopole (blue) and dipole (red) sources achieve perfect reflection, zero transmission and zero dissipated energy, whilst the pair of monopole sources (black) achieves zero transmission and reflection, and, therefore, perfect dissipation. Although the performance metrics are identical for the single monopole and dipole sources, the effective material properties are completely different, as shown in Figure 2. Both material properties are zero in the single monopole case, which corresponds to a pressure-release boundary condition. In the dipole case, both of the effective material properties tend towards infinity, which corresponds to a rigid boundary condition. The pair of monopole sources creates the perfect absorption condition by achieving an effective density equal to the ambient air density and zero bulk modulus. To provide further insight, the effective refractive index has been calculated and is presented in Figure 2f. This plot shows that the three active control systems create a refractive index that is greater than unity. A physical understanding of what the refractive index means in terms of the wave propagation can be gained by considering its definition, which is given by the ratio between the speed of sound and phase velocity, v_{phase}, of the incident waves, which is

$$n_{eff} = \frac{c_0}{v_{phase}}. \tag{11}$$

This indicates that the phase velocity across the secondary sources in all three cases presented in Figure 2 is slower than the speed of sound, but that in the case of the pair of monopole sources, where the refractive index is extremely large, the incident wave effectively stops.

4 OPTIMISATION PROCEDURES FOR DIRECT CONTROL OF THE EFFECTIVE MATERIAL PROPERTIES

It has been shown in the previous section how a traditional ANC strategy with various secondary source configurations influence the effective material properties and resulting wave propagation within a one-dimensional duct. In the context of AMMs there is a general objective to control the effective material properties directly.

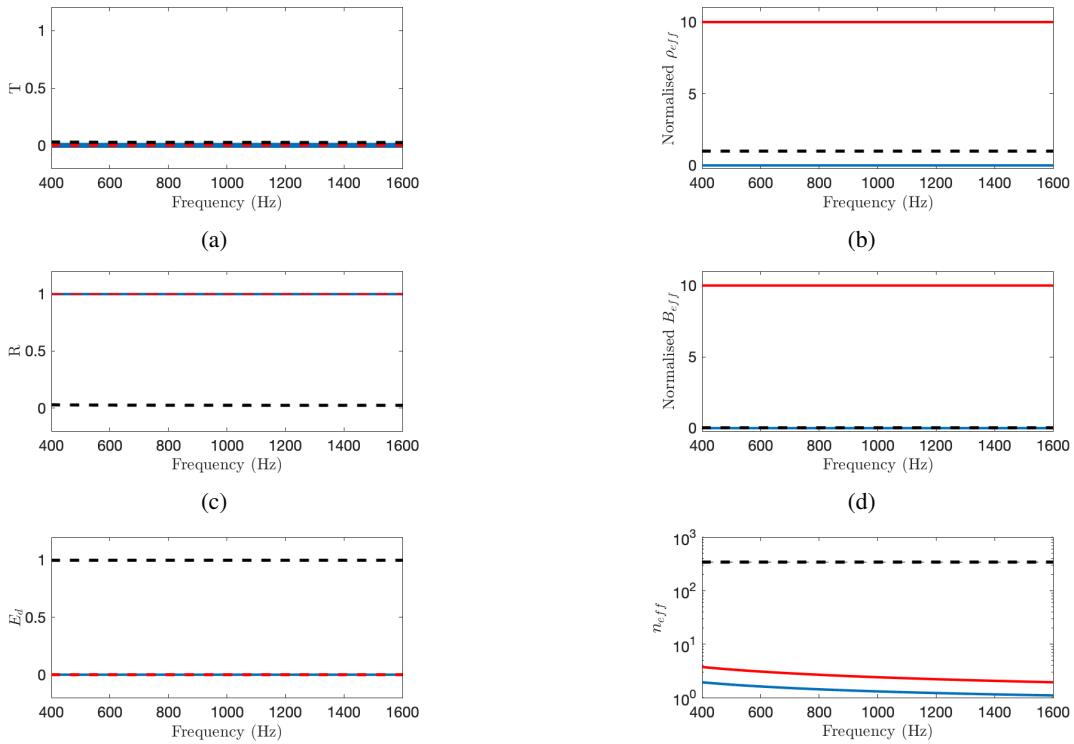

Figure 2. The performance of active control systems that are optimised to minimise the downstream pressure using a single monopole (blue), a dipole (red) and a pair of monopole (black) control sources. (a), (c) and (e) show the transmission and reflection coefficients and dissipated energy respectively and (b), (d) and (f) show the effective density, bulk modulus and refractive index respectively.

Therefore, this section presents an investigation into whether the secondary source configurations used in the previous section can be used to minimise the effective material properties directly. This is achieved using an optimisation procedure to achieve broadband negativity for the effective density and bulk modulus. Two cases have been considered in this study; a single monopole source that is driven to minimise the effective bulk modulus and a dipole source that is driven to minimise the effective density. In both cases, the optimisation procedure used the Globalsearch algorithm [21] in conjunction with the interior-point algorithm [22] to calculate the optimal source strengths numerically in Matlab, because it is not straightforward to calculate the optimal source strengths that minimise the effective material properties analytically. The Globalsearch algorithm has been implemented to increase the likelihood of obtaining the global minimum from the relatively complex cost surfaces associated with the effective material properties.

4.1 Results

The performance of the optimised monopole and dipole secondary sources has been evaluated using the transmission and reflection coefficients and dissipated energy, as well as the effective material properties and refractive index of the fluid medium, as described in Section 3.2. These metrics are shown in Figure 3 for the optimised systems. These results show that the single monopole source (blue) achieves transmission and reflection that both gradually increase over frequency, and negative dissipated energy. This indicates that the active control system is increasing the energy in the system and this can also be related to the transmission

being greater than unity. Figures 3b and 3d show that the single monopole source achieves negative effective bulk modulus over the frequency range of interest, demonstrating the effectiveness of the optimisation procedure, whilst the effective density is close to the ambient air density. Although, this optimised ANC configuration and the pair of monopole sources that are driven to minimise the downstream pressure generate the same effective density, the performance of each ANC strategy is completely different due to the bulk modulus in each case as shown in Figures 2d and 3d. The single monopole achieves an effective bulk modulus of around -2000 whilst the pair of monopole achieves zero bulk modulus. This shows that a large negative and zero bulk modulus coupled with a density close to the ambient air density will achieve perfect transmission and dissipation respectively.

To provide further insight into the physical behaviour of the single monopole achieving a negative bulk modulus and a density that is close to the ambient air density, the effective refractive index has also been calculated and is presented in Figure 3f. This result shows that the optimised single monopole source produces a near-zero refractive index. According to Eq. 11, it can be seen that this result is achieved by the phase velocity across the secondary source tending towards infinity, which not only leads to perfect transmission, but the transmitted waves will also experience minimal phase change.

From Figure 3, it can be seen that the dipole source optimised to minimise the effective density (red) achieves a transmission coefficient that approaches zero, a reflection coefficient that approaches one and, therefore, close to zero dissipated energy; this is similar to the result presented in Figure 2 when a dipole secondary source is driven to minimise the downstream pressure. However, it can also be seen from Figure 3 that the optimsed dipole source achieves negative effective density whilst the effective bulk modulus in this case is strictly positive, with a small positive value; this is distinct from the dipole source driven to minimise the downstream pressure, which exhibits both positive density and bulk modulus. As in the single monopole case, the effective refractive index has been calculated to provide further insight into the physical behaviour of the dipole source optimised to achieve negative density and this is presented in Figure 3f. It can be seen that the optimised dipole source produces a refractive index that is greater than unity, which means that the phase velocity across the control source must be slower than the speed of sound. This is similar to the dipole driven to minimise the downstream pressure, however, the differences in the effective material properties result in different magnitudes of the real and imaginary parts of the refractive index.

5 CONCLUSIONS

Active control is a well-developed technology that provides high performance noise control at low frequencies whilst maintaining a lightweight and compact package. In recent years, similar levels of noise control can be achieved using AMMs by achieving negative or zero effective density and bulk modulus. Active control has been combined with AMMs to improve the performance, tuneability and adaptability of the materials, however, the effects of active control on the effective material properties and wave propagation have not been extensively investigated. Therefore, this paper has investigated the effective material properties of a traditional ANC system in a one-dimensional duct using a single monopole, dipole and pair of monopole sources. The effective refractive index was also calculated to provide insight into how these active systems manipulate wave propagation in a one-dimensional environment.

In addition, this paper has also investigated whether these secondary source configurations can be used to directly minimise the effective material properties using an optimisation procedure and might thus be used as a metamaterial building block. It has been shown that the single monopole source can be optimised to achieve a negative bulk modulus and the dipole source can be optimised to achieve a negative density over the frequency range of interest. These results are consistent with prior literature in AMMs that state that a monopole source can create the monopole resonances required to achieve negative effective bulk modulus and a dipole source can create the dipole resonances required to achieve negative effective density. It has also been shown that the optimised single monopole source also achieves near-zero refractive index, which leads to perfect transmission with minimal phase change. The use of these monopole and dipole sources may, therefore, be utilised as unit

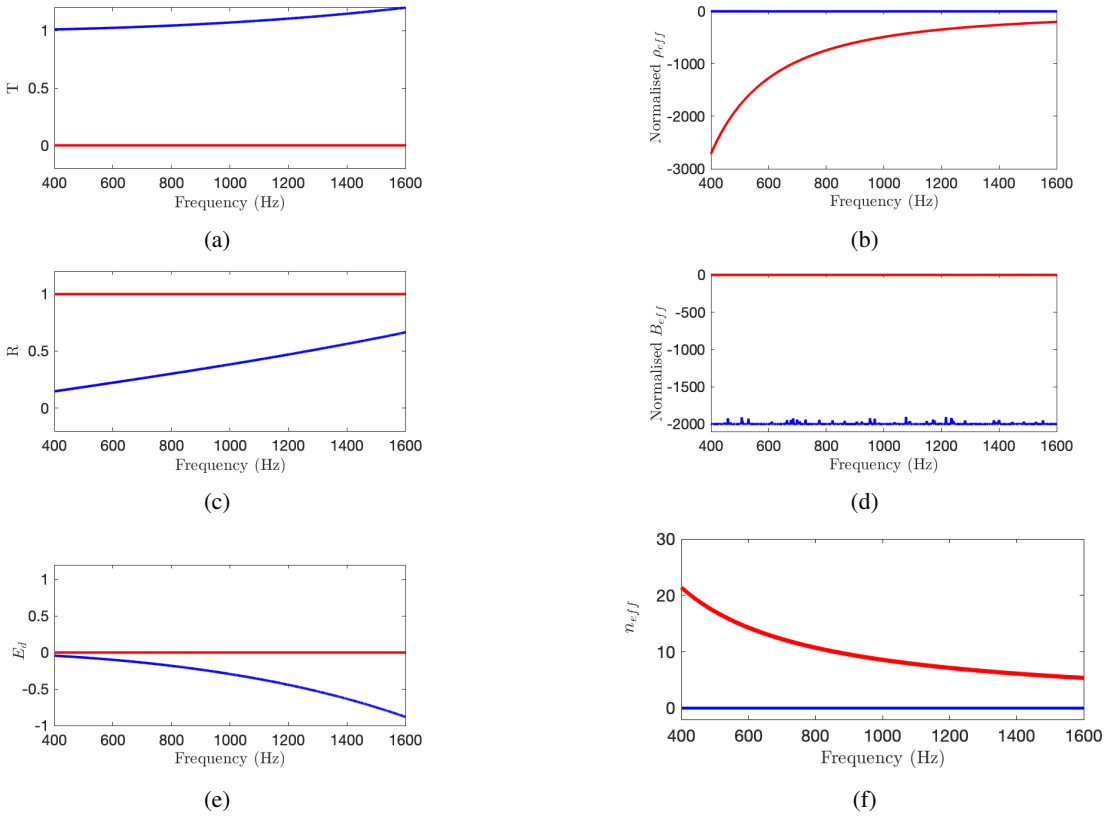

Figure 3. The performance of the single monopole (blue) and the dipole (red) sources that are driven to minimise the effective bulk modulus and density respectively. (a), (c) and (e) show the transmission and reflection coefficients and dissipated energy respectively and (b), (d) and (f) show the effective density, bulk modulus and refractive index respectively.

cells in the development of broadband single negative active acoustic metamaterials.

ACKNOWLEDGEMENTS

This research was partially supported by an EPRSC iCASE studentship (Voucher number 17000146) and an EPSRC Prosperity Partnership (EP/S03661X/1).

REFERENCES

[1] Yun Jing, Jun Xu, and Nicholas X. Fang. Numerical study of a near-zero-index acoustic metamaterial. *Phys. Lett. A*, 376(45):2834–2837, oct 2012.

[2] Zixian Liang and Jensen Li. Extreme Acoustic Metamaterial by Coiling Up Space. *Phys. Rev. Lett.*, 108(11):114301, mar 2012.

[3] Z. Yang, Jun Mei, Min Yang, N. H. Chan, and Ping Sheng. Membrane-type acoustic metamaterial with negative dynamic mass. *Phys. Rev. Lett.*, 101(20):1–4, 2008.

[4] Sam Hyeon Lee, Choon Mahn Park, Yong Mun Seo, Zhi Guo Wang, and Chul Koo Kim. Acoustic metamaterial with negative density. *Phys. Lett. Sect. A Gen. At. Solid State Phys.*, 373(48):4464–4469, 2009.

[5] Sam Hyeon Lee, Choon Mahn Park, Yong Mun Seo, Zhi Guo Wang, and Chul Koo Kim. Acoustic Metamaterial with Negative Modulus. *J. Phys. Condens. Matter*, 21(17), 2009.

[6] Chang Lin Ding and Xiao Peng Zhao. Multi-band and broadband acoustic metamaterial with resonant structures. *J. Phys. D. Appl. Phys.*, 44(21), 2011.

[7] Yiqun Ding, Zhengyou Liu, Chunyin Qiu, and Jing Shi. Metamaterial with simultaneously negative bulk modulus and mass density. *Phys. Rev. Lett.*, 99(9):2–5, 2007.

[8] Sam Hyeon Lee, Choon Mahn Park, Yong Mun Seo, Zhi Guo Wang, and Chul Koo Kim. Composite acoustic medium with simultaneously negative density and modulus. *Phys. Rev. Lett.*, 104(5):1–4, 2010.

[9] Nadège Kaina, Fabrice Lemoult, Mathias Fink, and Geoffroy Lerosey. Negative refractive index and acoustic superlens from multiple scattering in single negative metamaterials. *Nature*, 525(7567):77–81, 2015.

[10] Jong Jin Park, Choon Mahn Park, K. J. B. Lee, and Sam H. Lee. Acoustic superlens using membrane-based metamaterials. *Appl. Phys. Lett.*, 106(5):051901, feb 2015.

[11] Shu Zhang, Chunguang Xia, and Nicholas Fang. Broadband acoustic cloak for ultrasound waves. *Phys. Rev. Lett.*, 106(2):1–4, 2011.

[12] Choonghee Jo and Il Kwon Oh. A revisit to imperfect acoustic cloak of multi-layered shell structures considering sound speed and impedance matching. *J. Sound Vib.*, 333(19):4637–4652, 2014.

[13] M. Reynolds and S. Daley. *Active Control of Viscoelastic Metamaterials*. PhD thesis, University of Southampton, 2015.

[14] Bogdan Ioan Popa, Lucian Zigoneanu, and Steven A. Cummer. Tunable active acoustic metamaterials. *Phys. Rev. B - Condens. Matter Mater. Phys.*, 88(2), 2013.

[15] J. Cheer, S. Daley, and C. McCormick. Feedforward control of sound transmission using an active acoustic metamaterial. *Smart Mater. Struct.*, 26(2), 2017.

[16] Jordan Cheer. Active control of scattered acoustic fields: Cancellation, reproduction and cloaking. *J. Acoust. Soc. Am.*, 140(3):1502–1512, 2016.

[17] Jordan Cheer and Stephen Daley. The Effects of Active Noise Control on the Effective Material Properties. *Int. Congr. Sound Vib.*, pages 1–8, 2017.

[18] Vladimir Fokin, Muralidhar Ambati, Cheng Sun, and Xiang Zhang. Method for retrieving effective properties of locally resonant acoustic metamaterials. *Phys. Rev. B*, 76(14):144302, oct 2007.

[19] Ahmed Allam, Adel Elsabbagh, and Wael Akl. Modeling and design of two-dimensional membrane-type active acoustic metamaterials with tunable anisotropic density. *J. Acoust. Soc. Am.*, 140(5):3607–3618, nov 2016.

[20] Zsolt Szabo, Gi-Ho Park, Ravi Hedge, and Er-Ping Li. A Unique Extraction of Metamaterial Parameters Based on Kramers–Kronig Relationship. *IEEE Trans. Microw. Theory Tech.*, 58(10):2646–2653, oct 2010.

[21] Zsolt Ugray, Leon Lasdon, John Plummer, Fred Glover, James Kelly, and Rafael Martí. Scatter Search and Local NLP Solvers: A Multistart Framework for Global Optimization. *INFORMS J. Comput.*, 19(3):328–340, aug 2007.

[22] Richard H. Byrd, Jean Charles Gilbert, and Jorge Nocedal. A trust region method based on interior point techniques for nonlinear programming. *Math. Program.*, 89(1):149–185, nov 2000.